

Theory of Deeply Virtual Compton Scattering off the Unpolarized Proton

Brandon Kriesten* and Simonetta Liuti†

Department of Physics, University of Virginia, Charlottesville, VA 22904, USA.

Using the helicity amplitudes formalism, we study deeply virtual exclusive electron photoproduction off an unpolarized nucleon target, $ep \rightarrow e'p'\gamma$, through a range of kinematics both in the fixed target setting with initial electron energies of 6 GeV, 11 GeV and 24 GeV, and for an electron ion collider. We use a reformulation of the cross section that brings to the forefront the defining features of the $ep \rightarrow e'p'\gamma$ process as a *coincidence scattering* experiment, where the observables are expressed as bilinear products of the independent helicity amplitudes which completely describe the process in terms of the electric, magnetic and axial currents for the nucleon. These different contributions to the cross section are checked against the Fourier harmonics-based formalism which has provided so far the underlying mathematical framework to study Deeply virtual Compton scattering and related experiments. Using theoretical model calculations of the twist-two generalized parton distributions, H , E , \tilde{H} and \tilde{E} , we uncover large discrepancies between the harmonic series and our proposed framework. Most importantly, these numerical differences appear in the intermediate Q^2 range which represents a sweet spot for extracting generalized parton distributions from data. Our findings cast a doubt on extracting physically meaningful information from experimental data within the theoretical framework of the harmonics series where the approximations for the t and Q^2 are not traceable or under control.

I. INTRODUCTION

Deeply Virtual Compton Scattering (DVCS) is measured through the exclusive process, $ep \rightarrow e'p'\gamma$, where, in the one photon exchange approximation, the virtual photon four-momentum squared, Q^2 , provides a hard scale for the process. Quantum Chromodynamics (QCD) factorization theorems allow us to single out the perturbative, short distance reaction from the non-perturbative, long distance matrix elements described in terms of generalized parton distributions (GPDs).¹ GPDs enter the observables encoded in Compton Form Factors (CFFs), or convolutions over the longitudinal momentum variable x , with complex QCD Wilson coefficient functions (see reviews in [4–6]). At leading order, four quark chirality conserving GPDs giving eight CFFs, describe all possible quark-proton polarization configurations, $P_q P_p = UU, LL, UT, LT$, allowed by parity conservation, time reversal invariance and charge conjugation. The eight CFFs appear simultaneously in all of the deeply virtual exclusive scattering experimental observables, independent of the specific beam-target polarization configuration. This poses a challenge for the extraction of CFFs from experiment which are affected by large theoretical uncertainties (see [6] for a detailed list of experiments).

In Ref.[7] we introduced a new theoretical formulation of the cross section for the $ep \rightarrow e'p'\gamma$ process in all polarization configurations for the incoming electron and proton target. The main goal of Ref.[7] was to provide an exact and complete calculation of all terms entering the

cross section, to disentangle and evaluate, in particular, the impact of order $1/Q$ and higher power corrections of kinematic and dynamical origin.

Focusing on the unpolarized target case, in this paper we illustrate how the complete calculation of the cross section leads to a more direct interpretation in terms of the electric, magnetic and axial current contributions to DVCS. In our approach, the BH-DVCS interference term of the $ep \rightarrow e'p'\gamma$ cross section exhibits a structure analogous to the cross section for ep elastic scattering (see *e.g.* Refs.[8, 9] and references therein), preserving the structure of the nucleon charge, magnetic, and axial current contributions to the cross section from the underlying helicity amplitudes configurations [10, 11].

Previous studies, referring in particular to the widely adopted formalism of Refs. [5, 12–15] (BKM), failed to recognize this structure. The BKM cross section is organized, instead, in terms of harmonics of the azimuthal angle, ϕ , and in kinematic powers of $1/Q$. On one side, the harmonics-based formalism presents the appealing aspect of associating a dominant harmonic for each observable, therefore providing a simplified framework for experimental measurements which was perhaps needed in the initial analyses in the HERMES era [16]. On the other hand, information on the physics content of the coincidence cross section is much needed at the present stage of Jefferson Lab @12 GeV analyses.

For example, in Ref.[13] the magnetic contribution containing the angular momentum related CFF combination, $H + E$, to the BH-DVCS interference term, was deemed as power-suppressed and not included in the leading order formula. In Ref.[14] this term was restored into the main formula, however its relative importance was underestimated since it appeared with approximated $1/Q$ dependent coefficients.

Our framework enables the development of a Rosenbluth separation technique for unpolarized scattering

* btk8bh@virginia.edu

† sl4y@virginia.edu

¹ proofs of factorization for deeply virtual exclusive processes can be found in [1–3]).

data as well as , therefore radically changing our view on DVCS data.

While our approach shares a common starting point with the initial studies performed in Refs.[17–19], our results are similar to the recent study in Refs.[20–22], broadly labeled as “finite t and target mass corrections”, in that we recognize the importance of kinematic contributions originating from the choice of reference frames where the QCD hadronic tensor and BH proton current are evaluated.

Further advantages of the new formalism are that it is covariant for the BH and DVCS terms, while deviations from Lorentz covariance appearing in the interference term can be kept track of at every step. The covariance aspect is extremely advantageous from the practical point of view, in writing code and for the development of simulations and pseudo-data. A striking example is given by the form of the BH unpolarized cross section which greatly simplifies when written in terms of the relevant invariant products.²

The work presented in this paper is organized in the following points:

- i*) we focus on the unpolarized cross section where most data are available;
- ii*) we discuss in detail the physics content of the expressions derived in Ref.[7], including the origin of the phase dependence, and the polarization configurations for both the twist two and twist three contributions (Section II);
- iii*) we perform a detailed numerical comparison with the formalism of BKM for the unpolarized cross section including the BH, DVCS and BH-DVCS interference terms. The comparison is valid up to twist three, using the same model calculation of the GPDs for both the presents paper’s and the BKM expressions. This ensures that the differences can be ascribed entirely to the formalism, (Section III). We cover a range of kinematic regions, from Jefferson Lab @6 GeV and @12 GeV, to a hypothetical energy value of 24 GeV fixed target configuration [23] to the EIC [24] and EIC [25].

We write our Conclusions and Outlook in Section IV.

II. UNPOLARIZED SCATTERING CROSS SECTION

The cross section for the deeply virtual photon electro-production process, $e(k_e) + p \rightarrow e'(k'_e) + p' + \gamma'(q')$, on an unpolarized proton, is derived from a coherent superposition of the DVCS and Bethe-Heitler (BH) amplitudes, where the BH contribution arises when the final photon is emitted from either the initial or final electron. It is therefore a competing mechanism to the DVCS process evaluated at low momentum transfer, $-t \ll Q^2$. One has,

$$\begin{aligned} \frac{d^5\sigma}{dx_{Bj}dQ^2d|t|d\phi} &= \Gamma |T|^2 = \Gamma |T_{BH} + T_{DVCS}|^2 \\ &= \Gamma (|T_{BH}|^2 + |T_{DVCS}|^2 + \mathcal{I}), \end{aligned} \quad (1)$$

the interference term, \mathcal{I} , being defined as,

$$\mathcal{I} = T_{BH}^* T_{DVCS} + T_{DVCS}^* T_{BH}, \quad (2)$$

where Γ is the flux factor, $Q^2 = -(k_e - k'_e)^2$, $t = \Delta^2 = (p' - p)^2$, $x_{Bj} = Q^2/2(pq)$, with $\nu = (pq)/M$, ϕ is the angle between the lepton and hadron planes, M being the proton mass. In this paper we focus on the cross section for either an unpolarized or a polarized electron scattering off an unpolarized nucleon which are respectively given by,

$$\sigma_{UU} = \sigma_{UU}^{BH} + \sigma_{UU}^{DVCS} + \sigma_{UU}^{\mathcal{I}} \quad (3)$$

$$\sigma_{LU} = \sigma_{LU}^{DVCS} + \sigma_{LU}^{\mathcal{I}} \quad (4)$$

The detailed structure of the BH, DVCS, BH-DVCS interference contributions to the cross sections in Eqs.(3),(4) given in Ref.[7] in the Born approximation, read,

$$\sigma_{UU}^{BH} = \Gamma |T_{BH}|^2 = \frac{\Gamma}{t^2} [A_{BH}(y, x_{Bj}, t, Q^2, \phi) (F_1^2 + \tau F_2^2) + B_{BH}(y, x_{Bj}, t, Q^2, \phi) \tau G_M^2] \quad (5)$$

$$\sigma_{UU}^{DVCS} = \frac{\Gamma}{Q^2(1-\epsilon)} \left\{ F_{UU,T} + \epsilon F_{UU,L} + \epsilon \cos 2\phi F_{UU}^{\cos 2\phi} + \sqrt{\epsilon(\epsilon+1)} \cos \phi F_{UU}^{\cos \phi} \right\} \quad (6)$$

$$\sigma_{LU}^{DVCS} = \frac{\Gamma}{Q^2(1-\epsilon)} (2h) \sqrt{2\epsilon(1-\epsilon)} \sin \phi F_{LU}^{\sin \phi} \quad (7)$$

$$\sigma_{UU}^{\mathcal{I}} = e_l \frac{\Gamma}{Q^2 |t|} \left\{ A_{UU}^{\mathcal{I}} \Re(F_1 \mathcal{H} + \tau F_2 \mathcal{E}) + B_{UU}^{\mathcal{I}} G_M \Re(\mathcal{H} + \mathcal{E}) + C_{UU}^{\mathcal{I}} G_M \Re \tilde{\mathcal{H}} + \frac{\sqrt{t_0 - t}}{Q} F_{UU}^{\mathcal{I}, tw3} \right\} \quad (8)$$

$$\sigma_{LU}^{\mathcal{I}} = e_l \frac{\Gamma}{Q^2 |t|} \left\{ A_{LU}^{\mathcal{I}} \Im(F_1 \mathcal{H} + \tau F_2 \mathcal{E}) + B_{LU}^{\mathcal{I}} G_M \Im(\mathcal{H} + \mathcal{E}) + C_{LU}^{\mathcal{I}} G_M \Im \tilde{\mathcal{H}} + \frac{\sqrt{t_0 - t}}{Q} F_{LU}^{\mathcal{I}, tw3} \right\}. \quad (9)$$

² Our result is consistent with a previous calculation presented in

terms of Mandelstam invariants Ref.[17–19].

where h is the electron helicity, e_l is the electron charge, $y = (qp)/(kp)$, $\tau = -t/4M^2$, t_0 is the minimum t value allowed by taking the transverse four-momentum transfer $\Delta_T \geq 0$; ϵ , the ratio of longitudinal to transverse virtual photon flux in DVCS is given by,

$$\epsilon \equiv \frac{1 - y - \frac{1}{4}y^2\gamma^2}{1 - y + \frac{1}{2}y^2 + \frac{1}{4}y^2\gamma^2}$$

F_1 and F_2 are the Dirac and Pauli form factors. The CFFs are defined, in the QCD factorization framework, as convolutions of the GPDs for each quark flavor, q , with the Wilson coefficients functions. At leading order we have for, $\mathcal{F}_q = (\mathcal{H}_q, \mathcal{E}_q)$, and $\tilde{\mathcal{F}}_q = (\tilde{\mathcal{H}}_q, \tilde{\mathcal{E}}_q)$, respectively,

$$\mathcal{F}_q(\xi, t) = \mathcal{C}(C^+ F_q) \equiv \int_{-1}^1 dx C^+(x, \xi) F_q(x, \xi, t), \quad (10)$$

$$\tilde{\mathcal{F}}_q(\xi, t) = \mathcal{C}(C^- \tilde{F}_q) \equiv \int_{-1}^1 dx C^-(x, \xi) \tilde{F}_q(x, \xi, t). \quad (11)$$

with the leading order coefficients functions given by,

$$C^\pm(x, \xi) = \frac{1}{x - \xi - i\epsilon} \mp \frac{1}{x + \xi - i\epsilon}. \quad (12)$$

The GPDs observe crossing symmetry relations with respect to $x \rightarrow -x$, which allow us to introduce valence (symmetric) and quark singlet (anti-symmetric) distributions (for a detailed discussion see Refs.[26, 27]). In DVCS the proton GPD is written in terms of the quark GPDs as,

$$H = \sum_q e_q^2 H_q \quad (13)$$

e_q being the quark charge. The neutron GPD can be obtained using isospin symmetry.

Although the full structure of the cross section was already given in Ref.[7], to facilitate data analyses and interpretations, we make the following observations:

- The BH cross section is cast in a form similar to ep elastic scattering. However, due to the additional photon radiated from the electron in either the initial or final state, the virtual photon exchanged with the target is aligned along Δ at an angle ϕ , and the kinematic coefficients, A_{BH} and B_{BH} , multiplying the form factors acquire a complicated dependence in ϕ Ref.[7]. A more physical interpretation of these terms can also be obtained by writing the coefficients combination,

$$\epsilon_{BH} = \left(1 + \frac{B_{BH}}{A_{BH}}(1 + \tau)\right)^{-1} \quad (14)$$

measuring the exchanged virtual photon's longitudinal polarization relative to the transverse. Notice that $\epsilon_{BH} \neq \epsilon$.

- The DVCS structure functions are bilinear functions of the CFFs multiplied by kinematic coefficients that are directly related to the helicity structure for the process. We introduced a similar notation as in Refs.[11, 28] defining $F_{UU,T}$, $F_{UU,L}$, $F_{UU}^{\cos\phi}$, $F_{UU}^{\cos 2\phi}$, and $F_{LU}^{\sin\phi}$, where the first and second subscript define the polarization of the beam and target, respectively, the third subscript defines the polarization of the virtual photon; the superscripts refer to the azimuthal angular dependence associated with each structure function. Notice the structure of the multiplicative factors in each structure function: $F_{UU,T}$ has no $\sqrt{t_0 - t}/Q$ factor and is therefore the dominant term at high Q^2 ; $F_{UU}^{\cos\phi}$, $F_{UU}^{\sin\phi}$ contain one helicity flip factor $\propto \sqrt{t_0 - t}/Q$; $F_{UU}^{\cos 2\phi}$ is a leading twist contribution associated with a double helicity flip and it is both proportional to $(t_0 - t)/M^2$, and suppressed by a factor α_S from the gluon coupling; finally, $F_{UU,L}$, containing only twist-three GPDs, is given by the product of two single-flip terms yielding a multiplicative factor of $(t_0 - t)/Q^2$.

What renders DVCS analyses complicated with respect to inclusive and semi-inclusive deep inelastic scattering (SIDIS) experiments, is that owing to the fact that the CFFs appear in quadratic form, different polarization configurations do not cancel out when forming the various beam-target polarization structures. For instance, $F_{UU,T}$, the unpolarized structure function, contains CFFs from all GPDs, $H, E, \tilde{H}, \tilde{E}$ (similar results are obtained for the other observables). On the contrary, in SIDIS one has a one to one correspondence between the beam-target polarization configurations and TMDs. For instance, the structure function $F_{UU,T}$ in SIDIS measures the convolution of f_1 and the corresponding unpolarized fragmentation function, D_1 , similarly, F_{LL} measures the convolution of g_{1L} and D_1 , and so on [28, 29].

- The BH-DVCS interference contribution is expressed in terms of linear combinations of products of CFFs elastic form factors, F_1 and F_2 , with the coefficients, $A_{UU}^{\mathcal{I}}$, $B_{UU}^{\mathcal{I}}$, $C_{UU}^{\mathcal{I}}$, which are functions of (y, x_{Bj}, Q^2, ϕ) . Similar to the DVCS contribution, there is no obvious connection between the various beam/target polarization configurations and the GPDs contributing to the structure functions. On the other hand, similar to the BH term, one can single out the contributions,

$$F_1 \mathcal{H} + \tau F_2 \mathcal{E}, \quad G_M(\mathcal{H} + \mathcal{E}), \quad G_M \tilde{\mathcal{H}},$$

where the electric and magnetic properties of the cross section are clearly separated out, and, in addition, one has the equivalent of an axial charge term. The latter appears similar to an equivalent contribution in parity violating elastic scattering. It is allowed here by parity conservation, due to the

A. Difference with previous formulations

In unpolarized scattering for coincidence processes it is expected that the magnetic contribution will appear

suppressed with respect to the electric one. We reiterate, however, that *suppressed does not mean subleading* in this case: developing a framework that emphasizes contributions dominating the high Q^2 limit will, therefore, lead to erroneous interpretations.

Similar to how the magnetic form factor contribution is not dropped in the analysis of elastic scattering experiments, even if multiplied by a smaller coefficient than for the electric form factor, the magnetic contribution should be kept in the exclusive photoproduction cross section. It is, in fact, the most interesting term of the unpolarized cross section. Since it contains the combination of CFFs, $\mathcal{H} + \mathcal{E}$, it brings us closer to grasping the holy grail of angular momentum [30]. While analyses conducted so far disregard this term, we hope that this paper will help galvanize efforts to extract it.

To summarize our approach, we reiterate that the cross section evaluation should not be based on a hierarchy of power suppressed terms of the type M^2/Q^2 , t/Q^2 but that the coefficients multiplying the electric, magnetic, and axial current contributions should be evaluated in their entirety since the twist expansion has no foundation here [7].

This represents our main point of departure from the

BKM harmonics-based formalism [12–14] which is still widely used to interpret deeply virtual exclusive experiments. BKM organize the cross section in harmonics in the azimuthal angle, ϕ , and, even in the extended version in Ref.[14], only terms that are dominant in inverse powers of Q^2 are taken into account.

Another difference is in the treatment of the twist three GPD contributions, written in detail below, which we define along the lines of the GPD decomposition of the correlation function of Ref.[31].

Finally, the only way to evaluate the differences with BKM is to perform numerical calculations, since we have no access to intermediate parts of the calculations that lead to the final expressions presented in [12–14]. Section III is dedicated to a thorough numerical comparison of the two formalisms, in various kinematic regimes.

B. Twist three

We discuss structure of the BH-DVCS interference term at twist three, in view of the fact that it contains GPDs describing orbital angular momentum [32, 33],

$$\begin{aligned}
F_{UU}^{\mathcal{I},tw3} = & A_{UU}^{(3)\mathcal{I}} \left[F_1 \left(\Re e(2\tilde{\mathcal{H}}_{2T} + \mathcal{E}_{2T}) - \Re e(2\tilde{\mathcal{H}}'_{2T} + \mathcal{E}'_{2T}) \right) + F_2 \left(\Re e(\mathcal{H}_{2T} + \tau\tilde{\mathcal{H}}_{2T}) - \Re e(\mathcal{H}'_{2T} + \tau\tilde{\mathcal{H}}'_{2T}) \right) \right] \\
& + B_{UU}^{(3)\mathcal{I}} G_M \left(\Re e\tilde{\mathcal{E}}_{2T} - \Re e\tilde{\mathcal{E}}'_{2T} \right) \\
& + C_{UU}^{(3)\mathcal{I}} G_M \left[2\xi(\Re e\mathcal{H}_{2T} - \Re e\mathcal{H}'_{2T}) - \tau \left(\Re e(\tilde{\mathcal{E}}_{2T} - \xi\mathcal{E}_{2T}) - \Re e(\tilde{\mathcal{E}}'_{2T} - \xi\mathcal{E}'_{2T}) \right) \right]
\end{aligned} \tag{15}$$

For a polarized electron beam we obtain a structure anal-

ogous to the unpolarized case, where the $\Re e$ parts of the CFFs are replaced with with the $\Im m$ parts, namely,

$$\begin{aligned}
F_{LU}^{\mathcal{I}} = & A_{LU}^{(3)\mathcal{I}} \left[F_1 \left(\Im m(2\tilde{\mathcal{H}}_{2T} + \mathcal{E}_{2T}) - \Im m(2\tilde{\mathcal{H}}'_{2T} + \mathcal{E}'_{2T}) \right) + F_2 \left(\Im m(\mathcal{H}_{2T} + \tau\tilde{\mathcal{H}}_{2T}) - \Im m(\mathcal{H}'_{2T} + \tau\tilde{\mathcal{H}}'_{2T}) \right) \right] \\
& + B_{LU}^{(3)\mathcal{I}} G_M \left(\Im m\tilde{\mathcal{E}}_{2T} - \Im m\tilde{\mathcal{E}}'_{2T} \right) \\
& + C_{LU}^{(3)\mathcal{I}} G_M \left[2\xi(\Im m\mathcal{H}_{2T} - \Im m\mathcal{H}'_{2T}) - \tau \left(\Im m(\tilde{\mathcal{E}}_{2T} - \xi\mathcal{E}_{2T}) - \Im m(\tilde{\mathcal{E}}'_{2T} - \xi\mathcal{E}'_{2T}) \right) \right]
\end{aligned} \tag{16}$$

The coefficients are given in Ref.[7].

The notation for the twist three GPDs is illustrated in Table I where we show along with our our notation, their quark-proton polarization configuration, the corresponding notation in the TMD sector, and the notation from Ref.[31] (see also Table I in Ref.[7]). The notation follows the one adopted for TMDs [29, 34], namely,

- H and f correspond to the vector coupling in the parametrization of the quark-proton correlation function

- \tilde{H} and g correspond to axial-vector coupling
- the \perp superscript indicates an unsaturated transverse momentum index in the correlation function's coefficient [32]
- the subscript $L(T)$ involves the amplitude for a longitudinally (transversely) polarized target.

GPD	$P_q P_p$	TMD	Ref.[31]
H^\perp	UU	f^\perp	$2\tilde{H}_{2T} + E_{2T}$
\tilde{H}_L^\perp	LL	g_L^\perp	$2\tilde{H}'_{2T} + E'_{2T}$
H_L^\perp	UL	$f_L^{\perp(*)}$	$\tilde{E}_{2T} - \xi E_{2T}$
\tilde{H}^\perp	LU	$g^{\perp(*)}$	$\tilde{E}'_{2T} - \xi E'_{2T}$
$H_T^{(3)}$	UT	$f_T^{(*)}$	$H_{2T} + \tau \tilde{H}_{2T}$
$\tilde{H}_T^{(3)}$	LT	g_T'	$H'_{2T} + \tau \tilde{H}'_{2T}$

TABLE I. Twist-three GPDs and their helicity content. In the first column we show the GPDs notation for this paper; the second column shows the quark and proton polarizations; the third column shows the analogous configurations in the TMD sector; finally, the fourth column shows the corresponding notation from Ref.[31]. The asterisk denotes naive T-odd twist-three TMDs (we define $\tau = \frac{t_0 - t}{4M^2}$).

C. Azimuthal angular dependence

The azimuthal angular, ϕ , dependence is a key feature of the cross section, appearing with different capacities in the description of the BH, DVCS, and BH-DVCS interference contributions. In electron scattering coincidence reactions the cross section assumes a characteristic dependence on the *phase*, ϕ , which originates from rotating the virtual photon polarization vector, $\varepsilon_\mu^{\Lambda_\gamma^*}$, from the leptonic to the hadronic plane (see *e.g.* Refs.[35, 36] and the detailed reiteration for deeply virtual scattering in Ref.[10, 11]). This dependence allows us in general to single out the contributions from the overlap of different transverse and longitudinal amplitudes (*e.g.* $\sigma_T, \sigma_{TT}, \sigma_{LT} \dots$) describing different physics content.

In the specific case of exclusive photoproduction, we distinguish between the BH, and DVCS processes. In BH there are only two structure functions, *i.e.* the proton elastic form factors, therefore, similar to elastic scattering we do not organize the cross section by writing out the various virtual photon polarization components. The dependence on ϕ is purely kinematic.

For the DVCS and BH-DVCS contributions we set the virtual photon for DVCS, q , along the z axis in the laboratory frame, while the virtual photon, Δ , for the BH process is along Δ , at an angle ϕ with respect to q .

As shown below, this mismatch results in a much more complicated dependence of the polarization vector products contributing to the cross section, generating substantial t and target mass corrections [7].

1. Phase dependence of pure DVCS contribution

The polarization vectors for the virtual photon of momentum q along the negative z -axis in the laboratory

frame are defined as,

$$\begin{aligned} \varepsilon^{\Lambda_\gamma^* = \pm 1} &\equiv \frac{1}{\sqrt{2}}(0; \mp 1, i, 0), \\ \varepsilon^{\Lambda_\gamma^* = 0} &\equiv \frac{1}{Q}(|\vec{q}|; 0, 0, q_0) = \frac{1}{\gamma}(\sqrt{1 + \gamma^2}; 0, 0, 1), \end{aligned} \quad (17)$$

Notice that the DVCS helicity amplitudes are evaluated in the CoM frame of the final photon-hadron system, which defines the hadron plane at an angle ϕ with respect to the lepton plane [7]. The cross section is evaluated by transforming to the lepton plane rotating the polarization vectors defining the helicity amplitude, $f_{\Lambda\Lambda'}^{\Lambda_\gamma^* \Lambda_\gamma}$, by $-\phi$ about the z axis. Another way to express this is that the lepton produces a definite helicity virtual photon which we take along the z axis in the lepton plane; however, the virtual photon's interaction with the target occurs in the hadron plane which is rotated through an azimuthal angle ϕ . The phase dependence of the DVCS contribution to the cross section is a consequence of such a rotation about the axis where the virtual photon lies [35, 37]. The ϕ rotation about the z -axis changes the phase of the transverse components, and leaves the longitudinal polarization vector unchanged as,

$$\varepsilon^{\Lambda_\gamma^* = \pm 1} \rightarrow \frac{e^{-i\Lambda_\gamma^* \phi}}{\sqrt{2}}(0, \mp 1, i, 0) \quad (19)$$

The ejected (real) photon polarization vectors read,

$$\begin{aligned} \varepsilon^{\Lambda'_\gamma = \pm 1} &\equiv \frac{1}{\sqrt{2}}(0; \mp \cos \theta \cos \phi + i \sin \phi, \\ &\mp \cos \theta \sin \phi + i \cos \phi, \pm \sin \theta), \end{aligned} \quad (20)$$

$\varepsilon^{\Lambda'_\gamma}$ in principle also undergoes a phase rotation, however, this phase rotation does not contribute to the cross section due to the completeness relation obtained summing over the physical (on-shell) states [38],

$$\sum_{\Lambda'_\gamma} \left(\varepsilon_\mu^{\Lambda'_\gamma}(q') \right)^* \varepsilon_\nu^{\Lambda'_\gamma}(q') = -g_{\mu\nu} \quad (21)$$

2. Phase dependence of BH-DVCS interference term

The same treatment described above is applied to the BH-DVCS interference term. Here the different polarizations allow us to distinguish the twist-two and twist-three terms as,

$$twist \quad 2 \rightarrow \sum_{\Lambda_\gamma^* = \pm 1} \left(\varepsilon_\mu^{\Lambda_\gamma^*} \right)^* \varepsilon_\nu^{\Lambda_\gamma^*} = \cos \phi g_{\mu\nu}^T - \sin \phi \varepsilon_{\mu\nu}^T \quad (22)$$

$$twist \quad 3 \rightarrow \left(\varepsilon_\mu^{\Lambda_\gamma^* = 0} \right)^* \varepsilon_\nu^{\Lambda_\gamma^* = 0} = g_{\mu\nu}^L \quad (23)$$

where $g_{\mu\nu}^L = g_{\mu\nu} - g_{\mu\nu}^T$, its relevant components being, $g_{00}^L = 1 + \nu^2/Q^2$, $g_{03}^L = g_{30}^L = \sqrt{\nu^2 + Q^2} \nu/Q^2$, and $g_{33}^L = \nu^2/Q^2$.

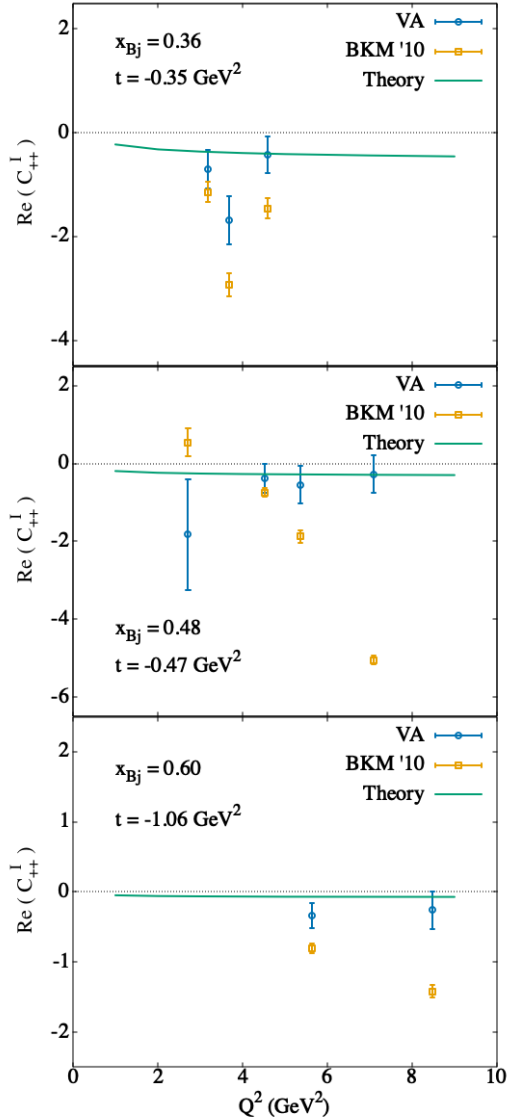


FIG. 1. The CFFs combination, C_{++}^I [14], plotted vs Q^2 . C_{++}^I is mostly sensitive to $F_1(t)\Re\mathcal{H}(\xi, t; Q^2)$, extracted from data [39] using the formalism presented in this paper and in Ref.[7] (blue diamonds), and using the formalism of Ref.[14] (orange squares). The curves in the figure illustrate the effect of perturbative QCD evolution, calculated using the GPD parametrization in Ref.[40].

In addition to the phase dependence, differently from the pure DVCS term where the azimuthal angular dependence resides entirely in the phase factors, the BH-DVCS contribution contains a ϕ dependence of kinematic origin. The kinematic ϕ dependence arises from the orientation of the Δ vector which lies at an angle ϕ in the hadronic plane and generates a ϕ dependence through factors of 4-vector products ($k\Delta$) in the coefficients of

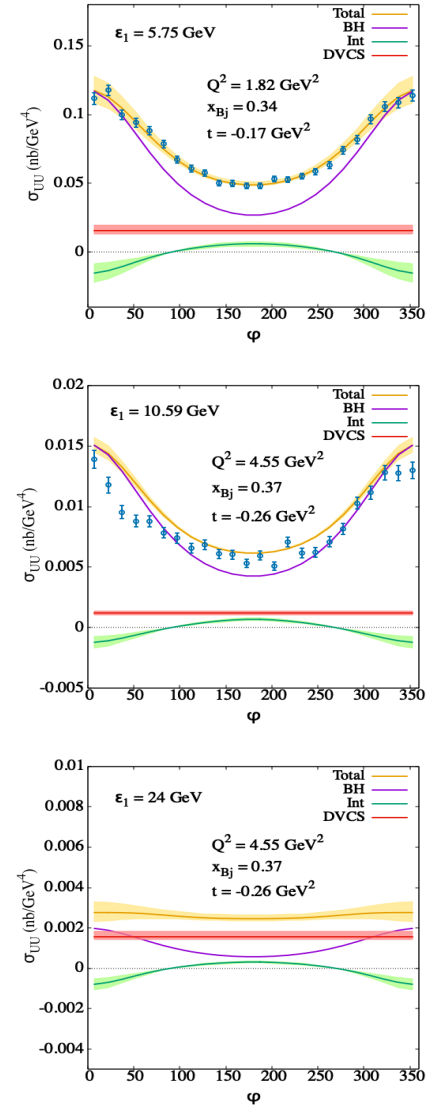


FIG. 2. The cross section σ_{UU} , Eq.(3) for the kinematic bins from Ref.[39] with initial electron energy $\epsilon_1 = 5.75$ GeV, $Q^2 = 1.8$ GeV², $t = -0.172$ GeV², $x_{Bj} = 0.34$ (top panel), Ref. [41] $\epsilon_1 = 11.5$ GeV, $Q^2 = 4.5$ GeV², $t = -0.29$ GeV², $x_{Bj} = 0.37$ (second panel), and for projected values of a fixed target experiment at $\epsilon_1 = 24$ GeV (third panel). The curves correspond to the contributions from: σ_{UU} Eq.(3), σ_{UU}^{BH} , (5), σ_{UU}^{DVCS} , (6), and σ_{UU}^I , (8), calculated in the laboratory system.

the structure functions similar to the BH case. As a result, we single out an overall multiplicative $\cos\phi$ term in the twist-two contribution to σ_{UU}^I , and a $\sin\phi$ term in the twist-two contribution to σ_{LU}^I , which originate from the phase dependence arising from the helicity amplitudes of the hadronic current. The coefficients contain also the kinematic ϕ dependence as explained above. A similar situation is found at twist-three where the phase dependence cancels out since for the virtual photon, $e^{-i\Lambda_\gamma \cdot \phi}$ is

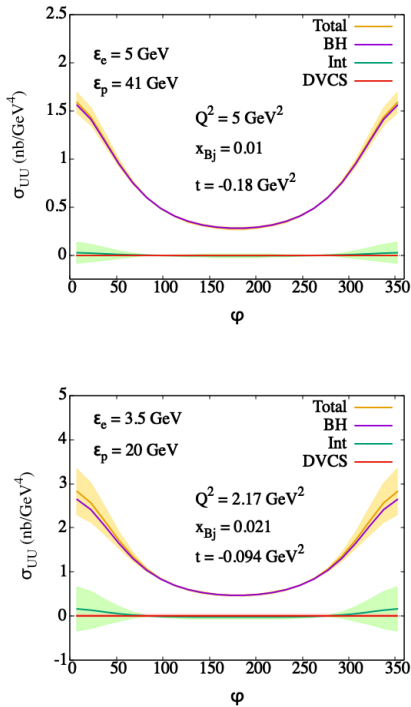


FIG. 3. The cross section σ_{UU} in a collider setting kinematics for an EIC with initial electron energy $\epsilon_e = 5$ GeV, initial proton energy $\epsilon_p = 41$ GeV, and kinematic bin $x_{Bj} = 0.01$, $t = -0.18$ GeV², and $Q^2 = 5$ GeV² of the US-based EIC [25] (top panel), and initial electron energy $\epsilon_e = 3.5$ GeV, initial proton energy $\epsilon_p = 20$ GeV, and kinematic bin $x_{Bj} = 0.021$, $t = -0.094$ GeV², and $Q^2 = 2.17$ GeV² of the China-based EIC [24] (bottom panel).

1 as a consequence of its longitudinal polarization, thus the ϕ dependence is entirely of kinematic origin.

This result seems at variance with the representation given in the original harmonics expansion of approach Refs.[13, 14]. However, one should notice that in these papers the distinction between the ϕ dependence from the phase of the polarization vectors and the ϕ dependence from the kinematics is not evident. This point of departure of the two formalisms is important as also addressed in Refs.[20–22], where the question of t and target mass corrections resulting from the different choices of the orientation of Δ has been also studied. In particular, it is important to establish a pathway in the decomposition of subleading twist terms which in our case clearly result from the ϕ -dependence from the “phase” of the hadronic current. This ensures that what enters into our twist-three cross section terms are directly due to twist-three GPDs and not to kinematically suppressed terms. These issues seem to have prevented so far a clean extraction of information from data [42].

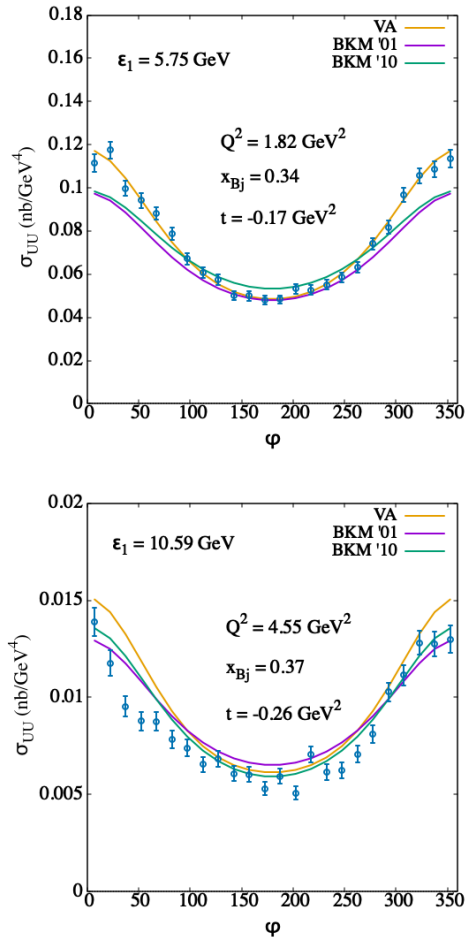


FIG. 4. Total Unpolarized Cross Section with VA theory CFF’s at kinematic bin *Left*: $Q^2 = 1.82$ GeV², $x_{Bj} = 0.34$, $t = -0.17$ GeV², $\epsilon = 5.75$ GeV and *Right*: $Q^2 = 4.55$ GeV², $x_{Bj} = 0.37$, $t = -0.26$ GeV², $\epsilon = 10.591$ GeV.

III. NUMERICAL RESULTS

In this Section we present numerical evaluations of the BH, DVCS and BH-DVCS interference terms evaluated in Ref.[7], emphasizing the feature of our new formalism as compared to previous approaches discussed in Section II.

We compare results obtained both in the helicity amplitudes and in the BKM formulations [13, 14], for various observables entering the unpolarized cross section at kinematic settings ranging from recent measurements at Jefferson Lab [39, 41], to a 24 GeV fixed target scenario [23], and the Electron Ion Collider (EIC) [24, 25]. Since the goal of this paper is to highlight the new features of the framework for exclusive electroduction as compared to BKM, we restrain from discussing issues involving fits to the cross section, the extraction of the CFFs from experimental data, and the modeling of GPDs based on DVCS data. These topics will be discussed in

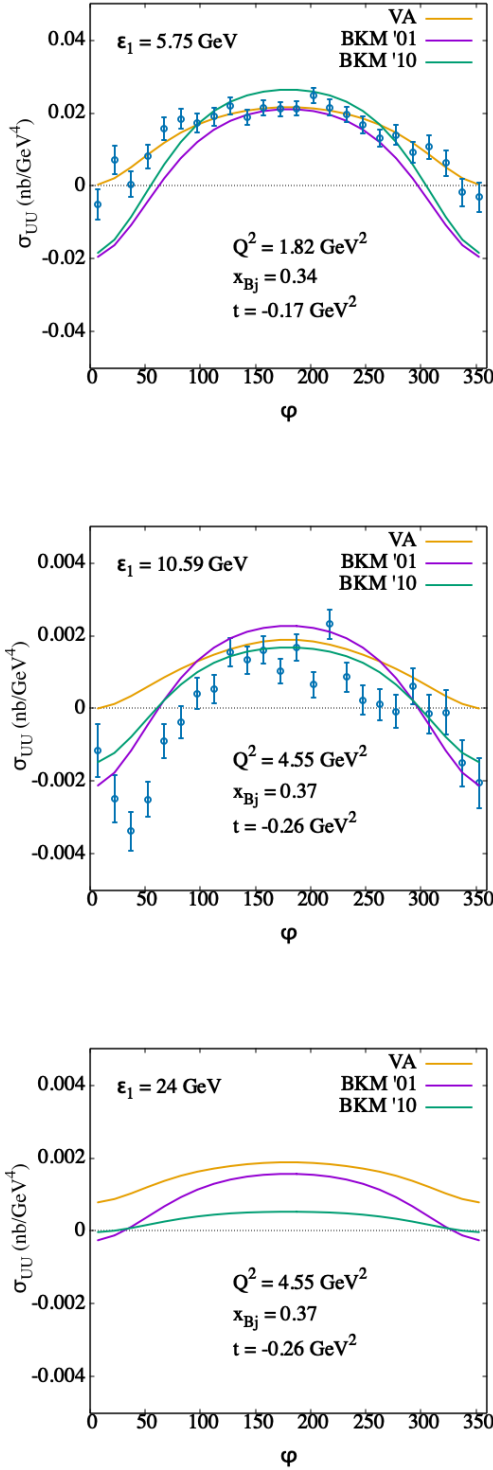


FIG. 5. Comparison of the interference cross section, σ_{UU}^I , Eq.(8), plus the DVCS cross section, σ_{UU}^{DVCS} , calculated using the frameworks from VA, BKM'01, BKM'10.

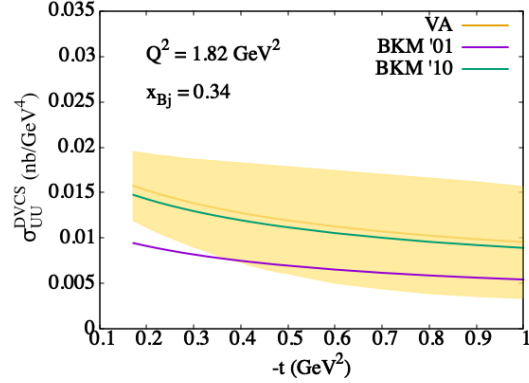


FIG. 6. Comparison of the unpolarized cross section, σ_{UU}^{DVCS} , Eq.(6), obtained in the VA and BKM frameworks, respectively. σ_{UU}^{DVCS} is plotted vs. $-t$ using the CFFs from the reggeized diquark model. The error band represents a theoretical error from the reggeized diquark model fit.

upcoming publications.

We start from showing in Figure 1 what is perhaps the biggest consequence of our new framework for deeply virtual exclusive scattering on an unpolarized proton: the dependence on the scale, Q^2 , of the BH-DVCS interference matrix element, labeled C_{++}^I , in Ref.[14], and dominated by the term $F_1(t)\mathcal{H}(x, \xi; Q^2)$. The extraction of this quantity in our formalism is consistent with a slow Q^2 dependence as predicted by the perturbative QCD evolution equations for GPDs [3, 26, 43]. In the BKM formalism, on the contrary, large oscillations appear which are the manifestation of a spurious Q^2 dependence resulting from the approximations taken in the cross section coefficients.

Notice that, although BKM use the harmonics based formulation where, in particular, the σ_{UU}^I cross section is not organized in terms of A_{UU}^I , B_{UU}^I , C_{UU}^I , one can retrieve equivalent expressions by rearranging the various harmonics contributions in Refs.[13, 14]. These expressions are displayed in the Appendix A. We note that even by doing so, the analytic comparison between the two formulations represents a formidable task due to the inherent complicated formalism. This further motivated our numerical comparison.

- In Figure 2 we present the cross section σ_{UU} , Eq.(3), with the separate contributions, σ_{UU}^{BH} , (5), σ_{UU}^{DVCS} , (6), and σ_{UU}^I , (8), calculated in the VA framework. We consider three different settings in the laboratory system with electron beam energies: $(k_e)_o = \epsilon_1 = 5.75, 11.5, 24$ GeV, and correspondingly increasing Q^2 values. The experimental data are from Ref.[39] (top panel) and Ref.[41] (middle panel). The 24 GeV setting [23] is becoming an exciting possibility that will allow further explorations of GPDs and the 3D structure of the nucleon in a wide kinematic range. In particular, the access to larger Q^2 values in the valence region will allow us to settle many

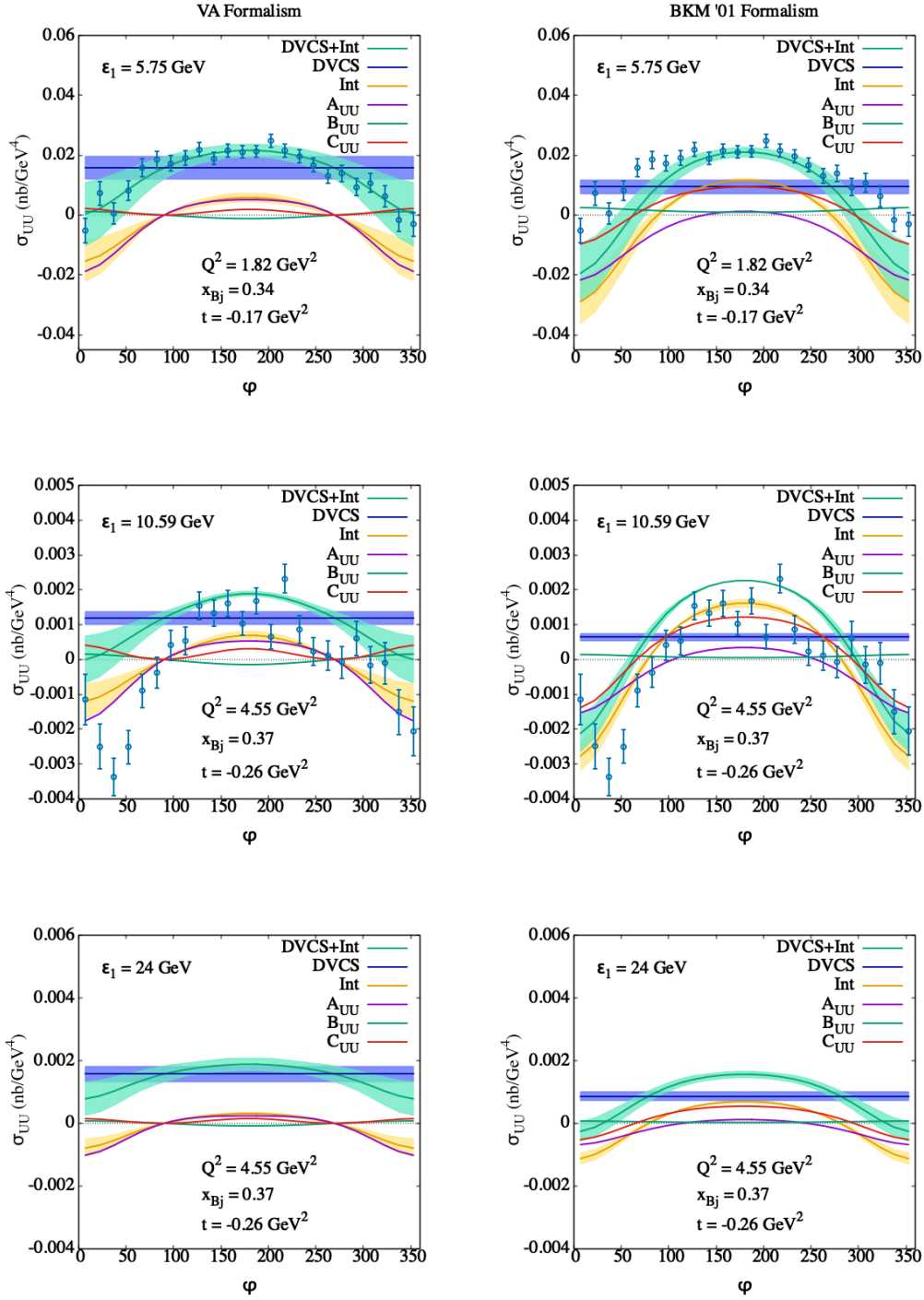


FIG. 7. BH-DVCS interference contribution to the cross section, σ_{UU}^I , Eq.(8) for initial electron energy $\epsilon_1 = 5.75$ GeV from Ref.[39] (top panel), $\epsilon_1 = 10.5$ GeV Ref.[41] (middle panel), and for a projected value of a fixed target experiment at $\epsilon_1 = 24$ GeV. The curves correspond to the calculation at twist-two using the reggeized diquark model [40] for the electric current which appears in the cross section multiplied by A_{UU} , the magnetic term with coefficient B_{UU} , and the axial term, C_{UU} .

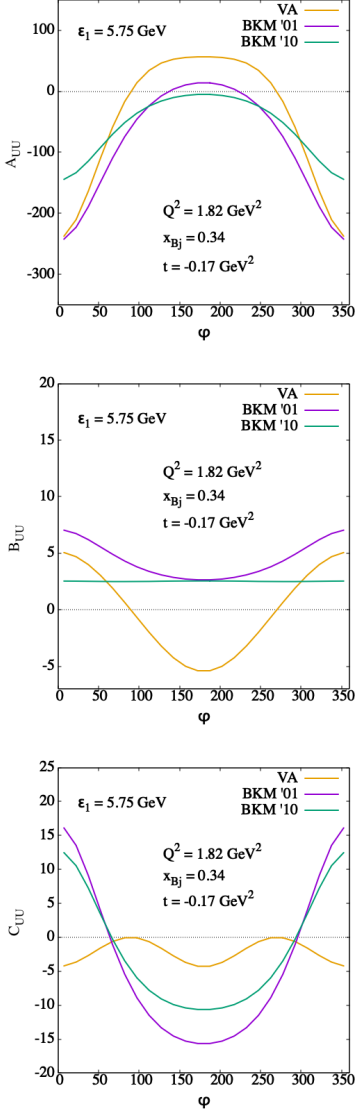


FIG. 8. Comparison of the kinematic coefficients, A_{UU} , B_{UU} , and C_{UU} , at the kinematics point $Q^2 = 1.82 \text{ GeV}^2$, $x_{Bj} = 0.34$, $t = -0.17 \text{ GeV}^2$, $\epsilon_1 = 5.75 \text{ GeV}$.

issues related to power corrections and the onset of QCD factorization. The theoretical predictions were calculated at leading twist using GPDs from the spectator model in [40, 44, 45], summarized in Section III A. We underline that these are predictions, namely the models parameters were fixed using constraints from experiments other than DVCS which include recent nucleon form factor and PDF measurements. The BH term is known to high precision, since its calculation is based on QED, the only unknowns being the nucleon form factors evaluated at low four-momentum transfer, t , where their uncertainty is small. The uncertainty band in the figure refers to the error from the fit obtained in [40, 44]. The same observables are shown in Figure 3 in collider settings [24, 25].

- In Figure 4 we compare the cross section obtained in the present framework (VA), and in the formulations of Refs.[13] (BKM'01) and Ref.[14] (BKM'10). All three calculations use the same CFFs evaluated in the reggeized diquark model, displayed in Table II. Although there are rather large discrepancies among the treatment of the DVCS contributions to the cross section in the three schemes, these appear minimized in the plots since the cross section is dominated by the BH contribution which is the same in both the VA and BKM formulations, despite the different expressions.

- The BH-DVCS interference term is shown Figure 5. The data were obtained by subtracting the BH contribution, which can be calculated exactly, and σ_{UU}^{DVCS} , Eq.(6), evaluated with the CFFs calculated in the reggeized diquark model (Table II). One can see clear discrepancies between the two frameworks, that do not seem to decrease with increasing electron energy. Differently from BKM, the VA formalism seems to capture features of the ϕ modulations characterizing the cross section at central values of ϕ .

- The DVCS cross section, σ_{UU}^{DVCS} , is plotted vs t in both the VA and BKM frameworks, in Figure 6, for the kinematic bin, $\epsilon_1 = 5.75 \text{ GeV}$, $Q^2 = 1.8 \text{ GeV}^2$, $x_{Bj} = 0.34$ (other kinematics display a similar trend). One can see that the improved calculation of Ref.[14] does bring the VA and BKM evaluations closer.

- To understand the origin of the discrepancies, in Figure 7 we examine the separate contributions to $\sigma_{UU}^{\mathcal{I}}$, Eq.(8), from $A_{UU}^{\mathcal{I}}(F_1\mathcal{H} + \tau F_2\mathcal{E})$, $B_{UU}^{\mathcal{I}} \propto G_M(\mathcal{H} + \mathcal{E})$, and $C_{UU}^{\mathcal{I}} \propto G_M\tilde{H}$. We juxtapose calculations using the VA formalism (left panels) to the BKM formalism (right panels). In the figure we also show σ_{UU}^{DVCS} , and the sum $\sigma_{UU}^{DVCS} + \sigma_{UU}^{\mathcal{I}}$ (the latter along with data obtained subtracting the BH term from the total cross section). What is striking is the different weight that the $A_{UU}^{\mathcal{I}}$, $B_{UU}^{\mathcal{I}}$, and $C_{UU}^{\mathcal{I}}$ terms carry in the VA and BKM frameworks, respectively. Furthermore, while the $A_{UU}^{\mathcal{I}}$ term dominates the VA cross section, the contribution from $C_{UU}^{\mathcal{I}}$ is important in the BKM case, especially with increasing energy. This represents the biggest discrepancy between the two approaches. The uncertainty bands in the figure are from the parametrization fit error [40].

- In Figures 8 and 9 we compare in detail the coefficients, $A_{UU}^{\mathcal{I}}$, $B_{UU}^{\mathcal{I}}$, $C_{UU}^{\mathcal{I}}$ in Eq.(8) for the two formulations. In Fig. 8 we show the coefficients in the kinematic bin, $\epsilon_1 = 5.7 \text{ GeV}$, $x_{Bj} = 0.34$, $-t = 0.17 \text{ GeV}^2$, $Q^2 = 1.8 \text{ GeV}^2$. One can see, first of all, substantial differences between the coefficients of the BKM'01 and BKM'10 definitions (especially for the magnetic contribution, $B_{UU}^{\mathcal{I}}$), that suggest that terms appear in the BKM'10 formulation, other than the power corrections $\propto 1/Q^2$. The differences with the VA formalism are even more striking, especially in the axial term, $C_{UU}^{\mathcal{I}}$, which is both smaller in size and it acquires more complex ϕ modulations in the VA case. These differences persist in the kinematic range of Jlab @ 12 GeV Ref.[41] (not shown in the figure). In order to understand whether the discrepancies are due

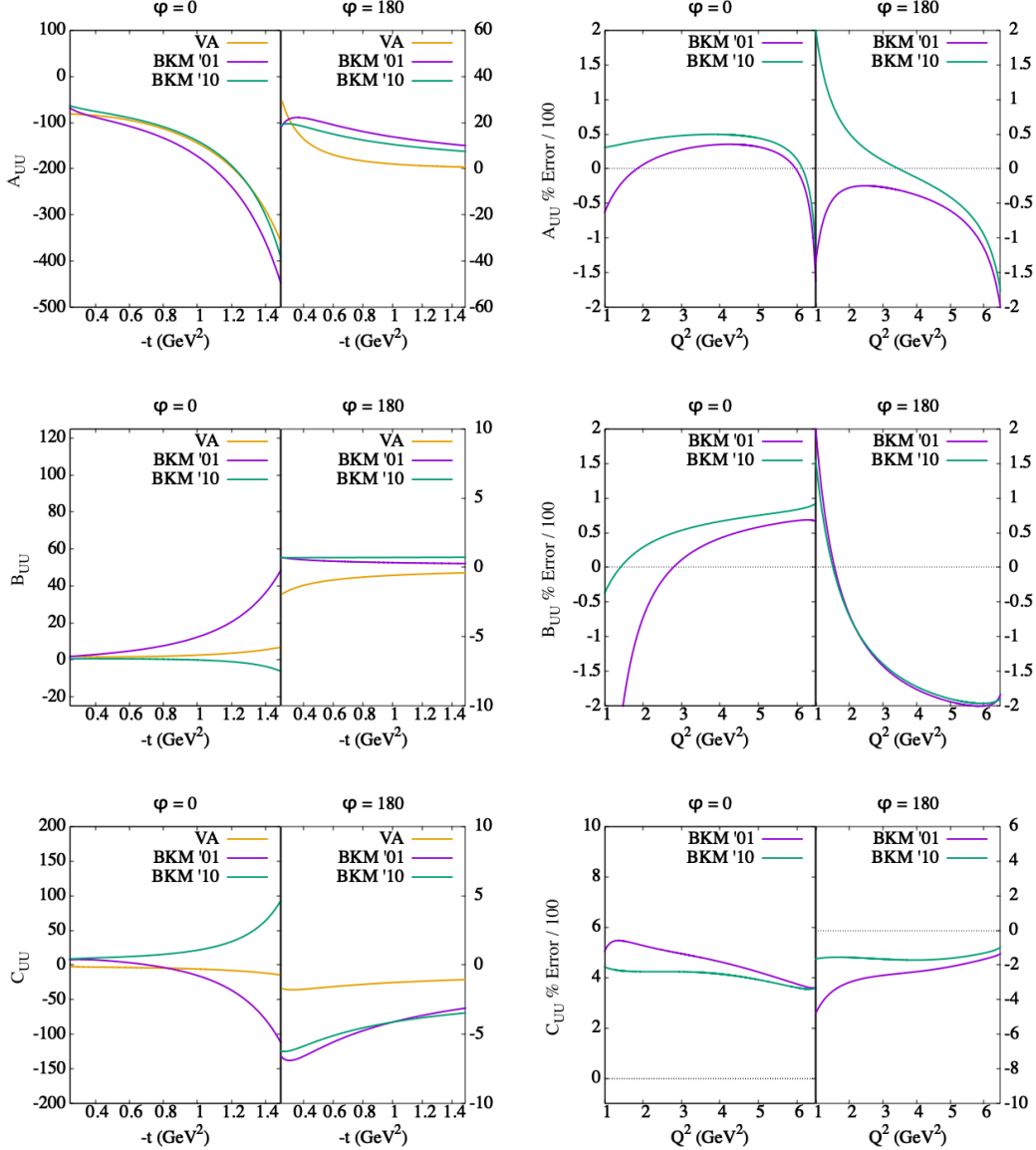


FIG. 9. Coefficients A_{UU}^T , B_{UU}^T , C_{UU}^T compared to the formulation from Ref.[13] (BKM'01) and [14] (BKM'10). On the left panels we show the coefficients for two kinematic settings: *Left*: $\epsilon_1 = 5.7$ GeV, $x_{Bj} = 0.34$, $Q^2 = 1.8$ GeV²; *Right*: $\epsilon_1 = 10.591$ GeV, $x_{Bj} = 0.34$, $-t = 0.17$ GeV²; on the right panels the percentage deviations between the BKM'01, BKM'10 calculations and the formalism presented in this paper are shown for the corresponding kinematics.

to terms proportional to M^2/Q^2 , t/Q^2 , we studied the behavior of the coefficients vs. t and Q^2 in the high Q^2 limit. The results shown in Figure 9 represent the coefficients, A_{UU} (top), B_{UU} (middle), and C_{UU} (bottom), evaluated at $\phi = 0$ (left panel) and $\phi = 180$ degrees (right panel). On the *lhs* we plot them as a function of $-t$, for the three frameworks BKM'01, BKM'10 and VA, at a lower value of $Q^2 = 1.8$ GeV²; on the *rhs* the percentage deviations of the BKM coefficients from the VA one are plotted vs. Q^2 at $-t = 0.17$ GeV². Notice that the differences among the approaches tend to subside at small t ,

while at large Q^2 substantial differences still persist. Our findings substantiate the hypothesis that the treatment of t -dependent and target mass corrections is important.

• Finally, in Figures 10, 11, we present our results for the polarized beam cross section, σ_{LU} , Eq.(4). In Fig. 10 we show the comparison with BKM'01 and BKM'10. Notice that with the VA formalism one can see that the twist-two CFFs do not describe quantitatively the cross section at $Q^2 = 1.8$ GeV², while the agreement improves increasing Q^2 to 4.5 GeV². Fig.11 displays the different contributions from the A_{LU}^T , B_{LU}^T , C_{LU}^T terms, Eq.(9).

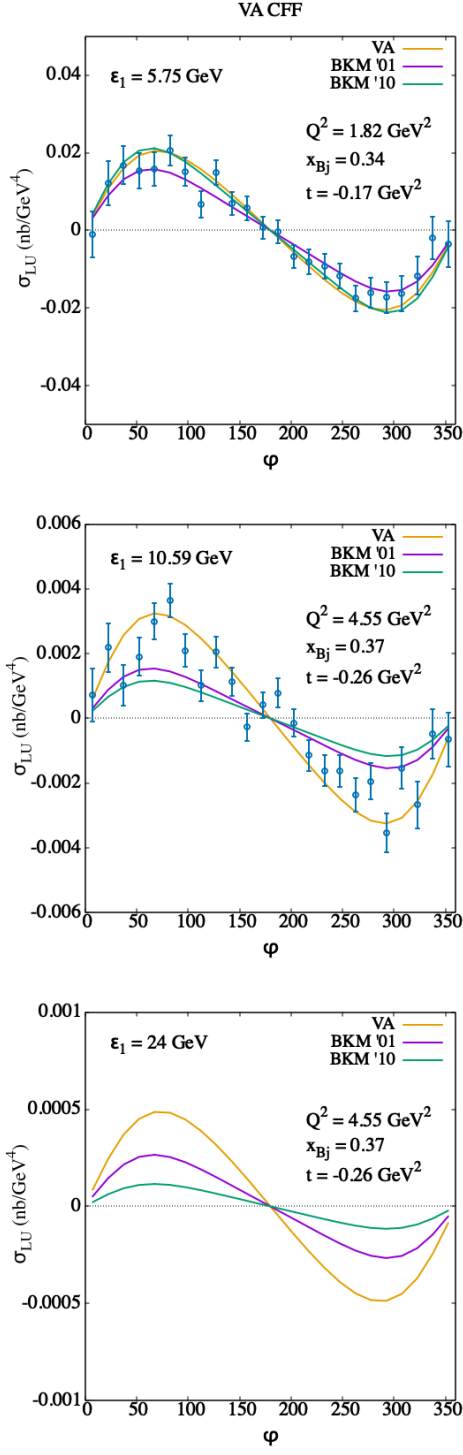


FIG. 10. Total LU Cross Section with VA theory CFF's at kinematic bin *Left*: $Q^2 = 1.82 \text{ GeV}^2$, $x_{Bj} = 0.34$, $t = -0.17 \text{ GeV}^2$, $\epsilon = 5.75 \text{ GeV}$ and *Right*: $Q^2 = 4.55 \text{ GeV}^2$, $x_{Bj} = 0.37$, $t = -0.26 \text{ GeV}^2$, $\epsilon = 10.591 \text{ GeV}$. Our prediction for a 24 GeV beam energy.

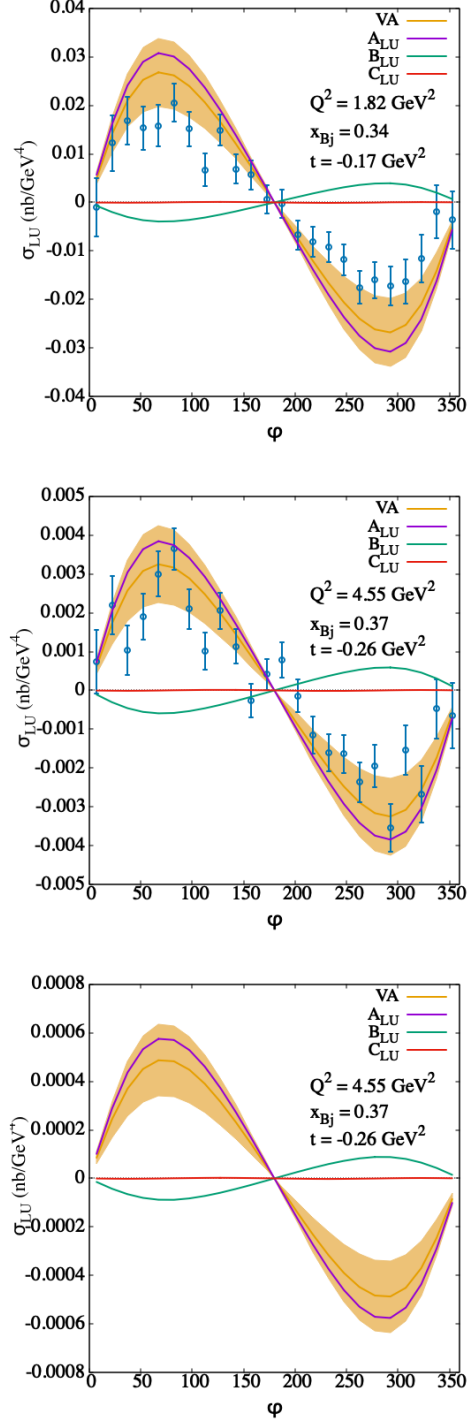


FIG. 11. Total LU Cross Section with VA theory CFF's at kinematic bin *Left*: $Q^2 = 1.82 \text{ GeV}^2$, $x_{Bj} = 0.34$, $t = -0.17 \text{ GeV}^2$, $\epsilon = 5.75 \text{ GeV}$ and *Right*: $Q^2 = 4.55 \text{ GeV}^2$, $x_{Bj} = 0.37$, $t = -0.26 \text{ GeV}^2$, $\epsilon = 10.591 \text{ GeV}$. Our prediction for a 24 GeV beam energy. Pieces of the cross section are shown.

Notice, in this case, the smallness of the axial contribution, $\propto G_M \mathfrak{S} m \tilde{H}$.

A. GPD Model

To compare the VA and BKM cross section frameworks we used the parametrization from Refs. [27, 40, 45] which is based on the reggeized diquark model. In the DGLAP region, $x > \xi$, the parametric form for $F_q = H_q, E_q, \tilde{H}_q, \tilde{E}_q$, at the initial scale $Q_0^2 \approx 0.1 \text{ GeV}^2$, reads,

$$F_q(x, \xi, t) = \mathcal{N}_q x^{[\alpha_q + \alpha'_q(1-x)^{p_q} t]} F_{diq}(x, \xi, t). \quad q = u, d \quad (24)$$

where F_{diq} , is obtained from a diquark calculation with mass parameters, m_q (quark mass), M_Λ (dipole cut-off mass), M_X^q (spectator diquark mass); $\propto x^{[\alpha_q + \alpha'_q(1-x)^{p_q} t]}$ accounts for the Regge behavior at low x . In the ERBL region, $-\xi < x < \xi$, we use a simple parametric form constrained by parity conservation and charge conjugation. The parameters for the twist-two GPDs are constrained from experimental data on the nucleon elastic form factors and PDFs, using:

i) the GPD normalization conditions,

$$\begin{aligned} \int_{-1}^1 H_q(x, \xi, t; Q^2) dx &= F_1^q(t), \\ \int_{-1}^1 E_q(x, \xi, t; Q^2) dx &= F_2^q(t) \\ \int_{-1}^1 \tilde{H}_q(x, \xi, t; Q^2) dx &= G_A^q(t) \\ \int_{-1}^1 \tilde{E}_q(x, \xi, t; Q^2) dx &= G_P^q(t), \end{aligned} \quad (25)$$

where we used the flavor separated data on the elastic nucleon form factors, F_1^q and F_2^q [46], and the nucleon axial [47] and pseudoscalar [48] form factor parametrizations;

ii) the forward limit conditions,

$$H_q(x, 0, 0; Q^2) = q(x, Q^2), \quad \tilde{H}_q(x, 0, 0; Q^2) = \Delta q(x, Q^2) \quad (26)$$

IV. CONCLUSIONS AND OUTLOOK

In order to extract information on the QCD matrix elements of deeply virtual exclusive electron scattering processes, one needs to first understand the detailed struc-

ture of the cross section. In deeply virtual exclusive photoproduction, in particular, tracking analytically the dependence in the high Q^2 limit on the invariants x_{Bj} and t , as well as on the angle ϕ between the lepton and hadron planes, has constituted a challenge which has been ham-

pered with the unpolarized PDF, $q(x)$, and the helicity distribution, $\Delta q(x)$, being evaluated using current nucleon PDFs parametrizations (details are in Refs.[49, 50]). To compare with data, the GPDs are perturbatively evolved at leading order to the scale, of the data, Q^2 [2, 3, 26, 43].

The values of the CFFs, $\mathcal{H}, \mathcal{E}, \tilde{\mathcal{H}}, \tilde{\mathcal{E}}$, corresponding to the measurements in [39] at $x_{Bj} = 0.34, 0.37$, $-t = 0.17, 0.26 \text{ GeV}^2$ and $Q^2 = 1.8, 4.5 \text{ GeV}^2$, are presented in Table II, compared with the values from the analyses in Refs.[51,

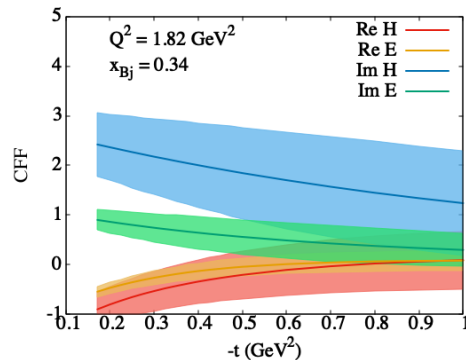


FIG. 12. VA Compton form factors H and E calculated in the reggeized diquark model, Eq.(24).

52]. Figure 12 shows the imaginary and real components of \mathcal{H} and \mathcal{E} in a similar kinematic range. The uncertainty bands in the figure represent the theoretical error of the parametrization [40].

Figure 13 illustrates how the values of the CFFs extracted from $\sigma_{UU}^T + \sigma_{UU}^{DVCS}$ using the BKM formalism in Ref.[51] (right panels) are far from fitting the data when inserted in the VA formulation (left panels). In other words, we see once more how the difference in formalism leads to substantially different CFFs values.

All values of the form factors used in the plots are displayed in Table II. Notice, in particular, that the value of the KM15 $\Re E$ contributing to σ_{UU}^{DVCS} , makes this term three times larger than our value.

Figure 14 shows a similar comparison to Fig.10, where now the CFFs are calculated using the model of [51, 52]. The model compares to the data using BKM'01 (a similar comparison is shown also in Ref.[39]).

ture of the cross section. In deeply virtual exclusive photoproduction, in particular, tracking analytically the dependence in the high Q^2 limit on the invariants x_{Bj} and t , as well as on the angle ϕ between the lepton and hadron planes, has constituted a challenge which has been ham-

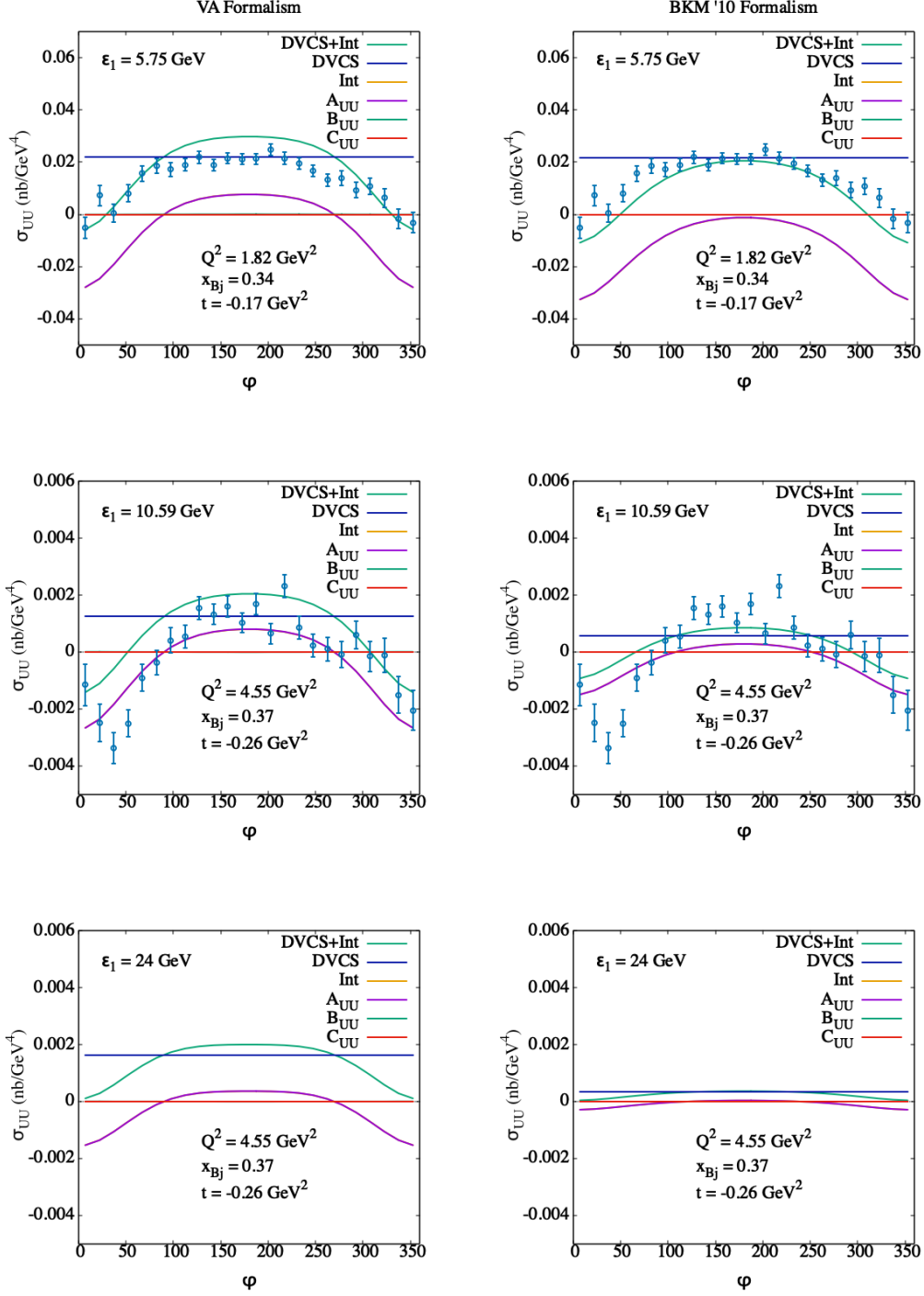


FIG. 13. Sum of contributions $\sigma_{UU}^T + \sigma_{UU}^{DVCS}$ using CFF values from Kumericki et al. [51] in two different formalisms for the cross section: VA formalism (left), BKM10 formalism (right).

pering, so far, a clean extraction of the various contributions to the cross section.

In our study, focusing on unpolarized scattering, we bring to the forefront features of the $ep \rightarrow e'p'\gamma$ process that define it as a *coincidence scattering* experiment, sin-

gling out the observables as bilinear products of the independent helicity amplitudes which completely describe the process. This structure is reflected in different ways in the DVCS and BH parts of the cross section.

For the BH process we obtain an expression similar

CFF	x_{Bj}	$-t$ (GeV ²)	Q^2 (GeV ²)	Re H	Re E	Re \tilde{H}	Re \tilde{E}	Im H	Im E	Im \tilde{H}	Im \tilde{E}
VA	0.34	0.17	1.82	-0.897	-0.541	2.444	2.207	2.421	0.903	1.131	5.383
VA	0.37	0.26	4.55	-0.884	-0.424	3.118	2.900	1.851	0.649	0.911	3.915
KM15	0.34	0.17	1.82	-2.254	2.212	1.399	141.362	3.506	-	1.565	-
KM15	0.37	0.26	4.55	-2.143	1.990	1.098	87.385	2.793	-	1.371	-
KM10a	0.34	0.17	1.82	-1.513	1.583	-	40.863	3.783	-	-	-
KM10a	0.37	0.26	4.55	-1.574	1.518	-	22.146	3.147	-	-	-

TABLE II. Value of Compton Form Factors using Virginia reggeized spectator model, global extraction from KM 15 [52] and KM 10a [51].

to elastic scattering experiments where the coefficients of the electric and magnetic proton elastic form factors squared acquire a ϕ dependence due to the emission of a real photon, and the tilt of the exchanged virtual photon off the lepton plane (along Δ). On the other hand, the DVCS contribution is described with the virtual photon, q , aligned along the z -axis, cast in a form similar to the semi-inclusive ep scattering process, where the various structure functions depend on bilinear combinations of CFFs multiplied by simple expressions in the variable ϵ (the longitudinal to transverse virtual photon polarization ratio). Twist-three contributions can be unambiguously separated out by the phase, ϕ , dependence. The DVCS-BH interference term formulation is driven by the BH amplitude. We have, in this case, in addition to the electric-type, $(F_1 - \tau F_2)(\mathcal{H} - \tau\mathcal{E})$ and magnetic-type, $(F_1 + F_2)(\mathcal{H} + \mathcal{E})$, contributions similar to the corresponding $(F_1 - \tau F_2)^2$ and $(F_1 + F_2)^2$ in the ep elastic scattering cross section, a third term, of the form $G_M \tilde{H}$. This term is allowed without violating parity conservation because of the extra degree of freedom provided by the outgoing photon along $q' \neq q$. The kinematic coefficients, as for the BH cross section, are lengthy but straightforward functions of ϕ evaluated to all orders in $1/Q$. In addition to this kinematic type ϕ dependence, a phase dependence on ϕ originates in a clearly distinguishable way, similar to the DVCS term. This distinction is important for the twist analysis in this and in related processes (*e.g.* time-like Compton scattering).

The new framework allows us to represent the interference cross section in a linear form in the CFF combinations, $\mathcal{H} - \tau\mathcal{E}$ and $\mathcal{H} + \mathcal{E}$, and to perform a Rosenbluth separation. A quantitative extraction of the CFFs from available data through such a linear fit of the reduced cross section will be presented in upcoming work.

Finally, we uncover substantial discrepancies with the harmonics decomposition of BKM, including the updated formulation with additional t/Q^2 and M^2/Q^2 terms. While the BH part of the cross section in our framework turns out to be numerically equivalent to the one in BKM, we find several discrepancies in both the pure DVCS, and DVCS-BH interference terms. These discrepancies are important and can affect considerably the extraction of CFFs from data, and consequently any conclusion on the behavior of angular momentum, pressure

or shear forces inside the proton. We tracked the differences between the BKM and VA formalism numerically, as a function of the various kinematic variables involved. We conclude that while the differences tend to be reduced at high Q^2 for some of the observables, this is not a general rule. The inherent reason behind the discrepancies is that in coincidence reactions, as it is well known from *e.g.* ep elastic scattering, one obtains misleading results by organizing the cross section coefficients according to their $t/Q^2 \rightarrow 0$ dependence, since this is not motivated in this case by the QCD twist expansion. As expected, making use of decades old experience in coincidence scattering experiments, the full Q^2 and t dependence needs to be considered. This is what our framework provides.

Our results might be compared in principle, with a more recent approach [20–22] which provides both the t -dependent and target mass corrections, albeit using the harmonics decomposition. Future work in this direction, including numerical evaluations of twist-three three CFFs, as well as an straightforward extension of our framework to timelike Compton scattering, will help us determine unambiguously the internal dynamics and mechanical properties of the proton.

ACKNOWLEDGMENTS

We thank SURA and Jefferson Lab for the support from the Center for Nuclear Femtography, and in particular to our colleagues participating in the University of Virginia lead initiative, Pete Alonzi, Matthias Burkardt (NMSU), Gordon Cates, Donal Day, Joshua Hoskins. We are also grateful to Jian-Ping Chen, Xu Cao and Yuxiang Zhao for discussing the projected EicC kinematic settings. Comments from Marie Boer, Markus Diehl and Charles Hyde are also gratefully acknowledged. This work was funded by DOE grants DOE grant DE-SC0016286 and in part by the DOE Topical Collaboration on TMDs (B.K. and S.L.).

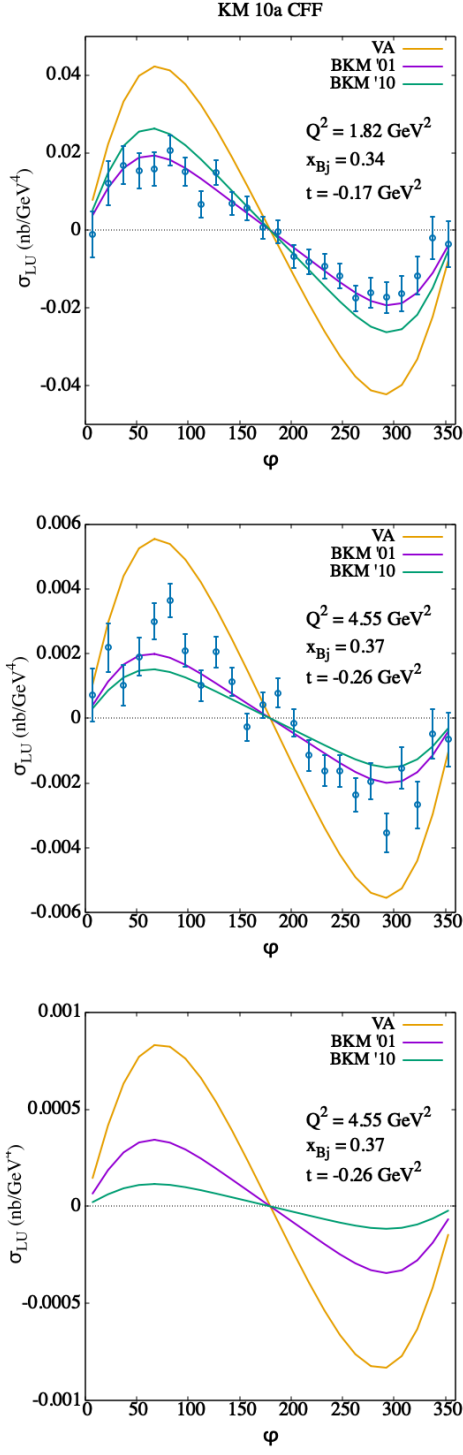


FIG. 14. Total LU Cross Section with Kumericki CFF's at kinematic bin *Left*: $Q^2 = 1.82 \text{ GeV}^2$, $x_{Bj} = 0.34$, $t = -0.17 \text{ GeV}^2$, $\epsilon = 5.75 \text{ GeV}$ and *Right*: $Q^2 = 4.55 \text{ GeV}^2$, $x_{Bj} = 0.37$, $t = -0.26 \text{ GeV}^2$, $\epsilon = 10.591 \text{ GeV}$. Our prediction for a 24 GeV beam energy.

Appendix A: BKM expressions for A_{UU}^Z , B_{UU}^Z and C_{UU}^Z

Shown are the coefficients A_{UU}^Z , B_{UU}^Z and C_{UU}^Z reevaluated using the expressions in Refs.[13, 14]

1. BKM Coefficients [13]

$$A_{UU}^Z = \frac{1}{x_{Bj}y^3t\mathcal{P}_1(\phi)\mathcal{P}_2(\phi)} \left\{ -8 \frac{(2-y)^3}{1-y} K^2 - 8(2-y) \frac{t}{Q^2} (1-y)(2-x_{Bj}) - 8K(2-2y+y^2) \cos(\phi) \right\} \quad (\text{A1})$$

$$B_{UU}^Z = \frac{\xi^2}{x_{Bj}y^3t\mathcal{P}_1(\phi)\mathcal{P}_2(\phi)} \left\{ 8(2-y) \frac{t}{Q^2} (1-y)(2-x_{Bj}) \right\} \quad (\text{A2})$$

$$C_{UU}^Z = \frac{\xi}{x_{Bj}y^3t\mathcal{P}_1(\phi)\mathcal{P}_2(\phi)} \left\{ 8 \frac{(2-y)^3}{(1-y)} K^2 + 8K(2-y+y^2) \cos(\phi) \right\} \quad (\text{A3})$$

where,

$$\mathcal{P}_1 = -\frac{1}{y(1+\gamma^2)} \{J + 2K \cos(\phi)\} \quad (\text{A4})$$

$$\mathcal{P}_2 = 1 + \frac{t}{Q^2} + \frac{1}{y(1+\gamma^2)} \{J + 2K \cos(\phi)\} \quad (\text{A5})$$

with,

$$K^2 = -\frac{t}{Q^2} (1-x_{Bj}) \left(1-y - \frac{y^2\gamma^2}{4}\right) \left(1 - \frac{t_0}{t}\right) \left\{ \sqrt{1+\gamma^2} + \frac{4x_{Bj}(1-x_{Bj}) + \gamma^2 t - t_0}{4(1-x_{Bj})} \frac{1}{Q^2} \right\} \quad (\text{A6})$$

$$J = \left(1-y - \frac{y\gamma^2}{2}\right) \left(1 + \frac{t}{Q^2}\right) - (1-x_{Bj})(2-y) \frac{t}{Q^2} \quad (\text{A7})$$

2. BKM'10 Coefficients [14]

$$A_{UU}^{\mathcal{I}} = \frac{1}{x_{Bj}y^3t\mathcal{P}_1(\phi)\mathcal{P}_2(\phi)} \left\{ \sum_{n=0}^3 C_{++}^{\text{unp}}(n) \cos(n\phi) \right\} \quad (\text{A8})$$

$$B_{UU}^{\mathcal{I}} = \frac{\xi}{x_{Bj}y^3t\mathcal{P}_1(\phi)\mathcal{P}_2(\phi)} \left\{ \sum_{n=0}^3 C_{++}^{\text{unp},V}(n) \cos(n\phi) \right\} \quad (\text{A9})$$

$$C_{UU}^{\mathcal{I}} = \frac{-\xi}{x_{Bj}y^3t\mathcal{P}_1(\phi)\mathcal{P}_2(\phi)} \left\{ \sum_{n=0}^3 \left(C_{++0}^{\text{unp},A}(n) + C_{++}^{\text{unp}}(n) \right) \cos(n\phi) \right\} \quad (\text{A10})$$

-
- [1] J. C. Collins and A. Freund, Phys. Rev. **D59**, 074009 (1999), arXiv:hep-ph/9801262 [hep-ph].
- [2] X.-D. Ji and J. Osborne, Phys. Rev. D **57**, 1337 (1998), arXiv:hep-ph/9707254.
- [3] X.-D. Ji and J. Osborne, Phys. Rev. D **58**, 094018 (1998), arXiv:hep-ph/9801260.
- [4] M. Diehl, Phys. Rept. **388**, 41 (2003), arXiv:hep-ph/0307382 [hep-ph].
- [5] A. Belitsky and A. Radyushkin, Phys.Rept. **418**, 1 (2005), arXiv:hep-ph/0504030 [hep-ph].
- [6] K. Kumericki, S. Liuti, and H. Moutarde, Eur. Phys. J. **A52**, 157 (2016), arXiv:1602.02763 [hep-ph].
- [7] B. Kriesten, S. Liuti, L. Calero-Diaz, D. Keller, A. Meyer, G. R. Goldstein, and J. Osvaldo Gonzalez-Hernandez, Phys. Rev. D **101**, 054021 (2020), arXiv:1903.05742 [hep-ph].
- [8] C. Perdrisat, V. Punjabi, and M. Vanderhaeghen, Prog. Part. Nucl. Phys. **59**, 694 (2007), arXiv:hep-ph/0612014.
- [9] H.-y. Gao, Int. J. Mod. Phys. **E12**, 1 (2003), [Erratum: Int. J. Mod. Phys.E12,567(2003)], arXiv:nucl-ex/0301002 [nucl-ex].
- [10] T. Arens, O. Nachtmann, M. Diehl, and P. V. Landshoff, Z. Phys. **C74**, 651 (1997), arXiv:hep-ph/9605376 [hep-ph].
- [11] M. Diehl and S. Sapeta, Eur. Phys. J. **C41**, 515 (2005), arXiv:hep-ph/0503023 [hep-ph].
- [12] A. V. Belitsky, D. Mueller, L. Niedermeier, and A. Schafer, Nucl. Phys. B **593**, 289 (2001), arXiv:hep-ph/0004059.
- [13] A. V. Belitsky, D. Mueller, and A. Kirchner, Nucl. Phys. **B629**, 323 (2002), arXiv:hep-ph/0112108 [hep-ph].
- [14] A. V. Belitsky and D. Mueller, Phys. Rev. **D82**, 074010 (2010), arXiv:1005.5209 [hep-ph].
- [15] A. V. Belitsky, D. Müller, and Y. Ji, Nucl. Phys. **B878**, 214 (2014), arXiv:1212.6674 [hep-ph].
- [16] M. Burkardt, C. Miller, and W. Nowak, Rept.Prog.Phys. **73**, 016201 (2010), arXiv:0812.2208 [hep-ph].
- [17] P. A. M. Guichon and M. Vanderhaeghen, Prog. Part. Nucl. Phys. **41**, 125 (1998), arXiv:hep-ph/9806305 [hep-ph].
- [18] M. Vanderhaeghen, P. A. Guichon, and M. Guidal, Phys. Rev. Lett. **80**, 5064 (1998).
- [19] M. Vanderhaeghen, P. Guichon, and M. Guidal, Nucl. Phys. A **654**, 602c (1999).
- [20] V. Braun and A. Manashov, JHEP **01**, 085 (2012), arXiv:1111.6765 [hep-ph].
- [21] V. Braun, A. Manashov, and B. Pirnay, Phys. Rev. Lett. **109**, 242001 (2012), arXiv:1209.2559 [hep-ph].
- [22] V. M. Braun, A. N. Manashov, D. Müller, and B. M. Pirnay, Phys. Rev. **D89**, 074022 (2014), arXiv:1401.7621 [hep-ph].
- [23] A. Bogasz, “https://www.jlab.org/accelerator-seminar-alex-bogacz-remote,” (2021).
- [24] D. P. Anderle *et al.*, (2021), arXiv:2102.09222 [nucl-ex].
- [25] R. A. Khalek *et al.*, (2021), arXiv:2103.05419 [hep-ph].
- [26] K. J. Golec-Biernat and A. D. Martin, Phys. Rev. D **59**, 014029 (1999), arXiv:hep-ph/9807497.
- [27] G. R. Goldstein, J. O. G. Hernandez, and S. Liuti, J.Phys. **G39**, 115001 (2012), arXiv:1201.6088 [hep-ph].
- [28] A. Bacchetta, M. Diehl, K. Goeke, A. Metz, P. J. Mulders, *et al.*, JHEP **0702**, 093 (2007), arXiv:hep-ph/0611265 [hep-ph].
- [29] P. Mulders and R. Tangerman, Nucl. Phys. **B461**, 197 (1996), arXiv:hep-ph/9510301 [hep-ph].
- [30] X.-D. Ji, Phys. Rev. Lett. **78**, 610 (1997), arXiv:hep-ph/9603249 [hep-ph].
- [31] S. Meissner, A. Metz, and M. Schlegel, JHEP **0908**, 056 (2009), arXiv:0906.5323 [hep-ph].
- [32] A. Rajan, M. Engelhardt, and S. Liuti, Phys. Rev. **D98**, 074022 (2018), arXiv:1709.05770 [hep-ph].
- [33] A. Rajan, A. Courtoy, M. Engelhardt, and S. Liuti, Phys. Rev. **D94**, 034041 (2016), arXiv:1601.06117 [hep-ph].
- [34] R. Jaffe and X.-D. Ji, Nucl.Phys. **B375**, 527 (1992).
- [35] S. Boffi, C. Giusti, and F. D. Pacati, Phys. Rept. **226**, 1 (1993).
- [36] T. W. Donnelly and A. S. Raskin, Annals Phys. **169**, 247 (1986).
- [37] V. Dmitrasinovic and F. Gross, Phys. Rev. **C40**, 2479 (1989), [Erratum: Phys. Rev.C43,1495(1991)].
- [38] R. Gastmans and T. Wu, *The Ubiquitous Photon* (Clarendon Press, Oxford, 1990).
- [39] M. Defurne *et al.* (Jefferson Lab Hall A), Phys. Rev. **C92**, 055202 (2015), arXiv:1504.05453 [nucl-ex].
- [40] J. O. Gonzalez-Hernandez, S. Liuti, G. R. Goldstein, and K. Kathuria, Phys. Rev. **C88**, 065206 (2013), arXiv:1206.1876 [hep-ph].
- [41] F. Georges, *Deeply virtual Compton scattering at Jefferson Lab*, Ph.D. thesis, Institut de Physique Nucléaire d’Orsay, France (2018).
- [42] M. Defurne *et al.*, Nature Commun. **8**, 1408 (2017), arXiv:1703.09442 [hep-ex].
- [43] I. Musatov and A. Radyushkin, Phys. Rev. D **61**, 074027 (2000), arXiv:hep-ph/9905376.
- [44] G. R. Goldstein, J. O. Gonzalez-Hernandez, and S. Liuti, Phys. Rev. **D84**, 034007 (2011), arXiv:1012.3776 [hep-ph].

- [45] B. Kriesten, P. Velie, E. Yeats, F. Y. Lopez, and S. Liuti, (2021), arXiv:2101.01826 [hep-ph].
- [46] G. D. Cates, C. W. de Jager, S. Riordan, and B. Wojtsekhowski, Phys. Rev. Lett. **106**, 252003 (2011), arXiv:1103.1808 [nucl-ex].
- [47] M. Schindler and S. Scherer, Eur. Phys. J. A **32**, 429 (2007), arXiv:hep-ph/0608325.
- [48] T. Gorringe and H. W. Fearing, Rev. Mod. Phys. **76**, 31 (2004), arXiv:nucl-th/0206039.
- [49] S. Ahmad, H. Honkanen, S. Liuti, and S. K. Taneja, Phys. Rev. D **75**, 094003 (2007), arXiv:hep-ph/0611046.
- [50] S. Ahmad, H. Honkanen, S. Liuti, and S. K. Taneja, Eur. Phys. J. C **63**, 407 (2009), arXiv:0708.0268 [hep-ph].
- [51] K. Kumericki, T. Lautenschlager, D. Mueller, K. Passek-Kumericki, A. Schaefer, and M. Meskauskas, (2011), arXiv:1105.0899 [hep-ph].
- [52] K. s. Kumericki and D. Müller, EPJ Web Conf. **112**, 01012 (2016), arXiv:1512.09014 [hep-ph].